

Land-Surface Model Development for the GISS GCM

CYNTHIA ROSENZWEIG

NASA/Goddard Institute for Space Studies, New York, New York

FRANK ABRAMOPOULOS

Science Systems and Applications, Incorporated and NASA/Goddard Institute for Space Studies, New York, New York

(Manuscript received 1 February 1995, in final form 4 September 1996)

ABSTRACT

A land-surface model is linked to the Goddard Institute for Space Studies (GISS) GCM Model II to form Model II-LS. The land-surface model primarily influences the simulation of surface air temperature over land, both in monthly means and diurnal range, and affects the major components of the hydrologic cycle over land—evapotranspiration, runoff, and, more indirectly, precipitation. Comparisons of January and July results of Model II-LS to results generated from the GISS GCM Model II and to observations show that the new land surface primarily provides improvements in the simulation of global evaporation and diurnal surface temperature range. The interannual variability of June–August surface air temperature in the Northern Hemisphere is also improved. When the land-surface model is combined with new parameterizations for moist convection and the planetary boundary layer, the combined version of the GCM yields improvements in evaporation. Simulations of a grassland site from an off-line version of the land-surface model compared to observations provided by the Project for Intercomparison of Land-Surface Parameterization Schemes of the Global Energy and Water Cycle Experiment show that the land-surface model simulates the ground temperature lag with depth in a reasonable way. Thus, the land-surface parameterization provides a more realistic simulation of climate variables over land in conjunction with other improvements to the GISS GCM.

1. Introduction

Land-surface model development for the Goddard Institute for Space Studies (GISS) general circulation model has two overlapping goals. The first is to improve the simulation of relevant fluxes to the atmosphere, especially latent and sensible heat fluxes. The second goal is to augment the physical realism of the land-surface component in order to facilitate the use of the model for earth system–global change studies, either in an independent mode or coupled with other process models. The land-surface model we are building at GISS could thus be used in the study of climate change, the effects of land degradation and deforestation on the hydrologic cycle, and the contribution of major river discharge to ocean salinity budgets.

In this paper, we describe aspects of a land-surface model (Model II-LS) that have been added since a previous paper (Abramopoulos et al. 1988), resulting from the linkage of the previous off-line model to the GISS GCM Model II (Hansen et al. 1983). This land-surface model differs from those developed by Dickinson

(1984) and Sellers et al. (1986), primarily in that the soil processes are more detailed, while the atmospheric connection is simpler. The GISS land-surface model conserves energy and water. It uses a canopy heat capacity instead of the flux balance approach used in many land-surface models to determine the canopy temperature; this simplifies the planetary boundary layer calculations and allows the heat of water intercepted on the canopy to be handled more easily.

We compare results of the new model to results generated from the previous GCM and to observations, and also to results of versions of the GISS GCM with new parameterizations for moist convection (Del Genio and Yao 1988, 1993; Del Genio et al. 1996) and the planetary boundary layer (Hartke and Rind 1996). The validation of the model improvements is discussed in Marango and Druyan (1994).

Results from a modified version of the GISS-LS (GISS-LS') are also presented. GISS-LS' has a lower canopy heat capacity and takes into account the effect of snow on canopy radiative fluxes. We show off-line GISS-LS' simulations of a grassland site compared to observations. This is part of the Project for Intercomparison of Land-Surface Parameterization Schemes (PILPS) of the Global Energy and Water Cycle Experiment (Henderson-Sellers and Dickinson 1992; Henderson-Sellers et al. 1995).

Corresponding author address: Dr. Cynthia Rosenzweig, Goddard Institute for Space Studies, 2880 Broadway, New York, NY 10025.
E-mail: crosenzweig@giss.nasa.gov

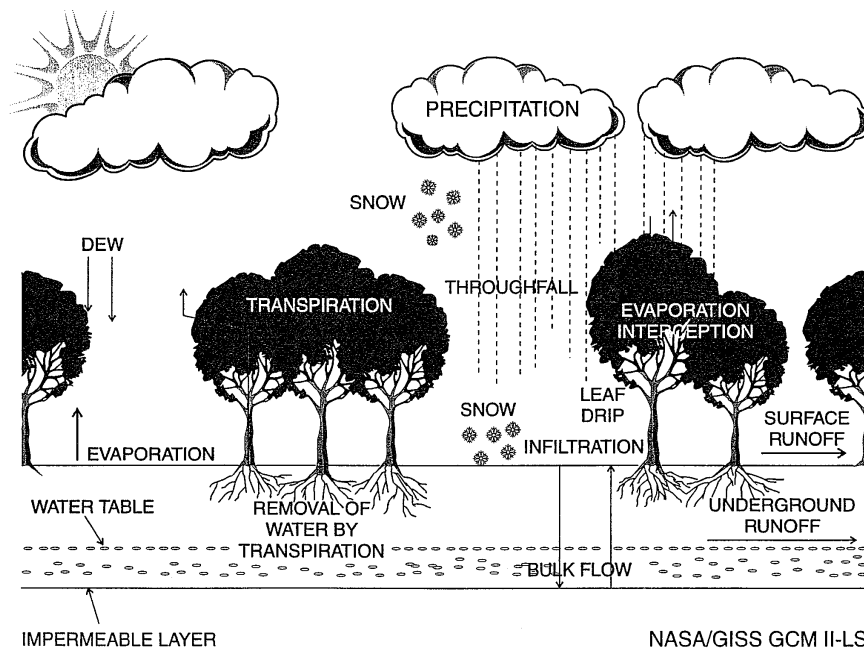


FIG. 1. Schematic representation of land-surface model processes.

2. Land-surface model

Modeled processes include infiltration, soil water flow, evaporation from bare soil, transpiration, evaporation from intercepted precipitation and dew, and throughfall (Fig. 1). Both surface and underground runoff are removed from the system. Precipitation and surface runoff are distributed at subgrid scales. The model accounts for frozen soil layers and snow on the canopy and soil. The model is one-dimensional for each grid box (Fig. 2). It divides the grid-box surface and the ground beneath it into bare and vegetated regions. These regions are conceptualized as interspersed. The vegetative canopy exists as a single layer with a heat capacity. The soil under both bare and vegetated regions is divided into six layers. Evaporative and heat fluxes are determined between the land surface and an atmospheric reference layer.

The land-surface model uses a forward time step. A one-half-hour time step is specified in the GCM for the land surface, but the land-surface model will switch to a shorter internal time step when needed to ensure stability.

a. Soil model

1) SOIL HEAT FLUX

The soil heat flux (F_H) is taken to be

$$F_H(z) = -K_H(z) \frac{dT(z)}{dz} + F_w(z)T(z)c_w, \quad (1)$$

where K_H is the soil thermal conductivity, T is the soil temperature, c_w is the specific heat capacity of water,

and z is the vertical coordinate. The first term represents heat conduction, and the second term is associated with the transport of heat due to water movement. The soil thermal conductivity is calculated as a function of water content using the method of De Vries (1966). The soil heat capacity is the volumetric average of the soil, water, and air heat capacities.

This equation is cast in finite difference form by using centered differences for the derivatives and by using the upstream temperature for the second term. The bottom boundary condition is set at zero flux. The specification of an impermeable bottom boundary conserves both heat and water in the model but does not allow the calculation of drainage to deep groundwater. The zero flux boundary condition tends to underestimate seasonal temperature lags in the soil.

2) SOIL TEMPERATURE, ICE, AND SNOW

The temperature of a soil layer is calculated from the heat in the layer and the heat capacity. If the layer includes ice, the heat of fusion h_f must be taken into account. The zero reference for heat is liquid water at 0°C. Here,

$$T_L = \begin{cases} H_L / (C_L + c_w W_L), & H_L > 0 \\ 0, & -h_f W_L \leq H_L \leq 0 \\ (H_L + h_f W_L) / (C_L + c_i W_L), & H_L < -h_f W_L, \end{cases} \quad (2)$$

where T_L is the temperature of a layer, H_L is the heat content of the layer, C_L is its heat capacity, W_L is the water content, and c_i is the specific heat capacity of ice.

The fraction of ice is given by

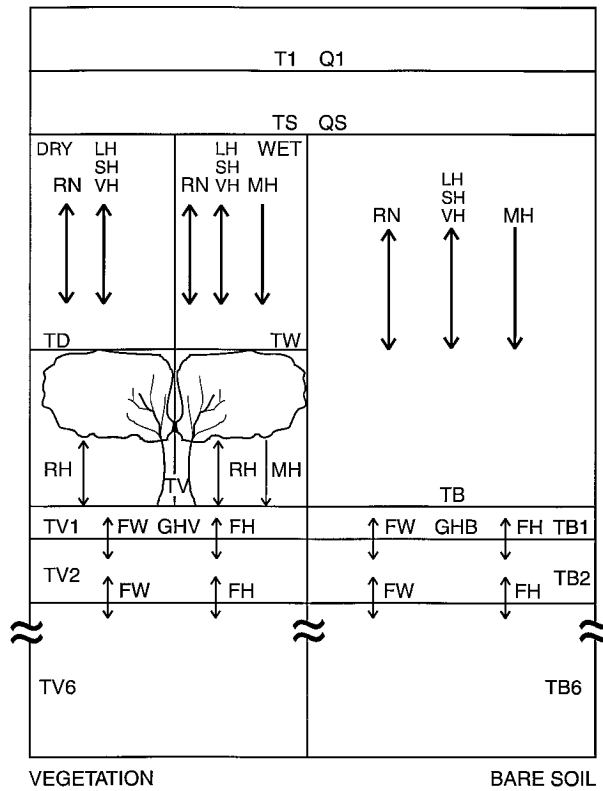


FIG. 2. Energy balance and temperature components of the land-surface model for coupling to the GISS GCM: RN—net radiation, LH—latent heat flux, SH—sensible heat flux, VH—heat of water vapor, MH—heat of water, TD—temperature of dry canopy, TW—temperature of wet canopy, RH—radiative heat between ground and canopy, TV—temperature of vegetated portion of land surface below canopy, TB—temperature of bare soil, TV1–6—temperatures of model soil layers of vegetated portion of land surface, FW—water flux between soil layers, GHV—heat flux into vegetated portion of land surface, FH—heat flux between soil layers, GHB—heat flux into bare soil, TB1–6—temperatures of model soil layers beneath bare soil portion of land surface, TS, QS—temperature and water vapor mixing ratio of surface layer, and T1, Q1—temperature and water vapor mixing ratio of first atmosphere layer.

$$\frac{I_L}{W_L} = \begin{cases} -\frac{H_L}{h_f W_L}, & T_L = 0 \\ 1, & T_L < 0 \\ 0, & T_L > 0, \end{cases} \quad (3)$$

where I_L is the quantity of ice in the layer.

To simplify model calculations, snow properties are embedded in the first ground layer. The water in the first soil layer W_1 includes liquid water, snow, and ice; the ice in the first soil layer I_1 includes both snow and ground ice. The heat of snow is also counted in the heat of the first soil layer H_1 . A separate prognostic variable S is the snow amount. The model limits the snow to be no more than the ice in the first layer. If ice in layer 1 melts, resulting in less ice than snow (i.e., $S > I_1$), then S is set equal to I_1 and the excess is added to the effective

precipitation used for surface runoff calculations. This has the effect of melting the first layer ground ice before melting the snow and may contribute to delayed snow-melt in the spring. Note that in the above, only W_L , H_L , and S are prognostic variables.

The effect of snow insulation is taken into account by combining the snow heat conductivity with the heat conductivity of the first layer soil. The heat conductivity of snow (set at $0.3 \text{ W m}^{-1} \text{ C}^{-1}$, as specified by Neeman et al. 1988) is usually less than the heat conductivity of soil, so this tends to reduce the overall heat conductivity of the first layer. Insulation reduces the heat flux between the first layer and the second layer due to the lower conductivity. However, the model cannot capture the effect of snow insulation within the first layer, which is important when the snow depth is large.

The snow is considered to cover a fraction of the canopy, cutting off transpiration from that fraction. The fraction depends on the vegetation height and is given by

$$f_s = 1 - \exp\left(-\frac{S}{V_h G_s}\right), \quad (4)$$

where f_s is the fraction of vegetation covered by snow, S is the water-equivalent snow depth, V_h is the vegetation height, and G_s is the specific gravity of snow.

3) SOIL FLUX LIMITS

Because the model does not include the hydrostatic potential, the finite difference formulation for the soil water fluxes is modified to prevent oversaturation in any layer by moving excess water to the layer above. If a positive flux is required at the first layer, it is added to the surface runoff.

b. Subgrid-scale precipitation and runoff

For bare soil, precipitation directly strikes the ground. For soil covered by vegetation, precipitation may first be intercepted by the canopy. Convective precipitation in the grid box is considered to fall only over a fraction f_p of the grid box; this fraction is currently specified at 10%, although it is known to vary regionally and seasonally (Eltahir and Bras 1993). Supersaturated precipitation is uniform in distribution. For convective precipitation, there are two mean precipitation values of relevance: one for the entire grid box (\bar{P}) and one for the fraction of the grid box over which precipitation is falling ($\langle P \rangle$). Within this fraction, the precipitation is assumed to have an exponential probability density function (Entekhabi and Eagleson 1989). The mean runoff for the grid box is then

$$\bar{R} = \bar{P} \exp(-f_p N / \bar{P}), \quad (5)$$

where N is the infiltration capacity.

Throughfall is also calculated at the subgrid scale.

The same assumptions are made for the throughfall and runoff calculations as for the precipitation distribution described above. Throughfall (P_v for precipitation under vegetation) is given by

$$P_v = \max(0, P - P_c), \quad (6)$$

where P_c is the maximum precipitation rate for which there is no throughfall; P_c is taken to be a fixed precipitation rate ($1 \times 10^{-6} \text{ m s}^{-1}$) times the fraction of the canopy that is dry. This formula states that there is no throughfall unless the precipitation rate is above a threshold level. The idea is that low-intensity rainfall has smaller droplets, which, when striking the leaves, are likely to be held to the leaves because of surface tension. High-intensity rainfall, on the other hand, has larger droplets with enough kinetic energy so that the surface tension cannot completely capture the water.

In addition to this type of throughfall, there is also the drip that occurs when the canopy water storage capacity is exceeded. Drip does not affect our subgrid-scale analysis, and so is not considered in what follows, although it is present in the model.

Mean throughfall for the region with precipitation is then

$$\bar{P}_v = \bar{P} \exp(-f_p P_c / \bar{P}). \quad (7)$$

c. Linking the land-surface model to the GCM

The land-surface model calculates the average ground temperature at each time step and passes it to the GCM surface routine; the GCM surface routine then returns the corresponding coefficient of drag and surface air temperature to the land-surface model. The aerodynamic method is used to calculate evaporation from the ground to the surface layer (30 m) for the bare and vegetated portions of the grid box. These separate components are combined, and the combined moisture flux is balanced with the flux from the surface layer to the first layer of the atmosphere. Fluxes are positive in the upward direction.

1) GROUND- AND FIRST-LAYER FLUXES

Sensible heat and evaporation fluxes from the bare and vegetated portions of the grid box are calculated using the aerodynamic formulation (Hansen et al. 1983). Distinct temperatures characterize the two portions.

The evaporation from the bare soil portion of the grid box is, as described in Abramopoulos et al. (1988), taken to be the minimum potential evaporation and the maximum amount of water that can evaporate from the top layer of soil based on the Gardner-Hillel diffusivity limit (Gardner and Hillel 1962; Hillel 1975) plus the precipitation. This limit implies a value of β_B , the evaporative efficiency over bare soil.

For evaporation occurring over the vegetated portion of the grid box, evaporation occurs at the potential rate

for the wet portion of the canopy. For the dry canopy, transpiration is determined by the canopy conductance (C_c) in series with the atmospheric conductance (C_a). Condensation of dew always occurs at the potential rate. Taken together, the evaporation for the wet and dry portions imply a value for β_v , the evaporative efficiency over the canopy.

The canopy conductance is determined from the minimal stomatal resistance r_s , the effective leaf area index L_{eff} , the incoming solar radiation I , the canopy temperature, and the soil water availability factor β_D , which depends on the matric potential in the soil and the root density:

$$C_c = \beta_D \frac{L_{\text{eff}}}{r_s} \frac{\left(\frac{I}{I + c_1}\right)}{1 + \left(\frac{T_c - c_2}{c_3}\right)^4}, \quad (8)$$

where T_c is the canopy temperature; c_1 , c_2 , c_3 are parameters, specified as 90 W m^{-2} , 23°C , and 15°C , respectively (B. Choudhury 1990, personal communication); and β_D is defined in Abramopoulos et al. (1988).

The sensible heat and moisture fluxes from the surface layer into the first layer of the atmosphere (F_{h1} and F_{q1}) are calculated by the diffusion formula (Hansen et al. 1983).

2) RADIATION RELATIONSHIPS

Over the bare soil portion of the grid box, the net radiation is the balance of the emitted longwave radiation with the absorbed incoming solar and the downward longwave radiation. For the vegetated portion of the grid box, the ground under the canopy exchanges heat via blackbody radiation with the canopy above. The canopy transmits neither shortwave nor longwave radiation. Radiation balances are calculated for both the ground under the canopy and the canopy layer.

3) SENSIBLE HEAT FLUX BALANCE AT THE SURFACE

The sensible heat flux from the ground to the surface is constrained to be equal to the sensible heat flux from the surface to the first layer of the atmosphere. This is so because the surface layer is taken to have zero thickness. The sensible heat flux from the ground to the surface is calculated as the area-weighted sum of the sensible heat fluxes from the bare soil and vegetated portions of the grid box:

$$F_{h1} = f_B F_{hB} + f_V F_{hV}, \quad (9)$$

where f_B is fraction of bare soil, $f_V = 1 - f_B$ is the vegetated fraction, F_{hB} is the sensible heat flux from bare soil, and F_{hV} is the sensible heat flux from the canopy. The sensible heat flux balance equation is

TABLE 1. Vegetation types and characteristics^a specified in GISS land-surface model.

	Tundra	Grassland	Shrub	Woodland	Deciduous	Evergreen	Rainforest
Minimum LAI ^a	1.0	1.0	1.0	1.0	1.0	8.0	6.0
Maximum LAI ^b	1.5	2.0	2.5	4.0	6.0	10.0	8.0
Minimum stomatal resistance ^c (s m ⁻¹)	100	100	200	200	200	300	250
Root depth (m)	0.1	1.1	1.5	2.0	2.0	2.0	0.8
Root coefficient a ^d	12.5	0.9	0.8	0.25	0.25	0.25	1.1
Root coefficient b ^d	1.0	0.9	0.4	2.00	2.00	2.00	0.4

^a Albedo, masking depth, and roughness length are specified as in Hansen et al. (1983). Land-cover fraction is calculated as in Matthews (1984) with the percentage of desert assumed to be equivalent to the percentage of bare soil.

^b Seasonal leaf area index (LAI) is specified as sine function between minimum and maximum LAI, with peak LAI occurring on day of year 196.

^c Functional coefficients relate stomatal resistance to solar radiation and temperature.

^d For use in the cumulative root distribution function $F(z) = az^b$.

$$C_a(f_B T_B + f_V T_C - T_S) = K \frac{T_S - T_1}{Z_1 - Z_S}, \quad (10)$$

where T_B is the temperature of bare ground, T_S is the temperature of the surface layer, T_1 is the temperature of the first layer of the atmosphere, K is the eddy diffusion coefficient, Z_S is the height of the surface layer, and Z_1 is the height of the first layer of the atmosphere.

The ground temperature (T_G) is the area-weighted sum of the bare ground and canopy temperatures:

$$T_G = f_B T_B + f_V T_C. \quad (11)$$

Substituting (11) into (10),

$$C_a(T_G - T_S) = K \frac{T_S - T_1}{Z_1 - Z_S}. \quad (12)$$

Thus, the area-weighted flux of sensible heat is the same as the flux derived from the area-weighted ground temperature based on a single heat transfer coefficient for the entire grid box. Because the overall flux can be treated as the result of a single ground temperature, (12) can be solved for T_S , as well as C_a and K , with the GISS Model II surface routine.

4) MOISTURE FLUX BALANCE AT THE SURFACE

The moisture flux from the ground to the surface must also equal the flux from the surface to the first layer of the atmosphere (F_{q_1}). The moisture flux from the ground to the surface is calculated as the area-weighted sum of the moisture fluxes from the bare soil and vegetated portions of the grid box:

$$F_{q_1} = f_B F_{q_B} + f_V F_{q_V}, \quad (13)$$

where F_{q_B} is the moisture flux from bare soil and F_{q_V} is the moisture flux from the canopy. Explicitly,

$$\begin{aligned} & f_B \beta_B C_a (q_B - q_S) + f_V \beta_V C_a (q_C - q_S) \\ &= K \frac{q_S - q_1}{Z_1 - Z_S}, \end{aligned} \quad (14)$$

where q_B is the saturated water vapor mixing ratio at the temperature of the bare soil, q_C is the saturated water

vapor mixing ratio at the temperature of the canopy, q_S is the water vapor mixing ratio at the surface layer, and q_1 is the water vapor mixing ratio in the first layer of the atmosphere.

In the case of the moisture flux balance at the surface, the area-weighted fluxes cannot be calculated as a single flux from the area-weighted mixing ratio. This is because there are different efficiency factors (β) for the bare and vegetated portions of the grid box. Thus,

$$q_S = \frac{f_B \beta_B C_a q_B + f_V \beta_V C_a q_C + K q_1 / (Z_1 - Z_S)}{f_B \beta_B C_a + f_V \beta_V C_a + K / (Z_1 - Z_S)}. \quad (15)$$

This equation is used to solve for q_S by successive approximation.

5) ENERGY BALANCE AT THE CANOPY

The rate of change of the canopy heat (H_C) is the sum of all the heat fluxes into the canopy,

$$\frac{dH_C}{dt} = R_{nC} - F_{hV} - \lambda F_{qV} + F_{hP} - F_{hd}, \quad (16)$$

where R_{nC} is the net radiation of the canopy, λ is the latent heat of vaporization, F_{hP} is the heat flux carried by precipitation, and F_{hd} is the heat flux carried off by throughfall.

The temperature of the canopy is given by

$$T_C = \begin{cases} H_C / (c_W W_C + C_D), & \text{if } 0 < H_C \\ 0, & \text{if } -h_f W_C \leq H_C \leq 0 \\ (H_C + h_f W_C) / (c_f W_C + C_D), & \text{if } H_C < -h_f W_C, \end{cases} \quad (17)$$

where W_C is the water on the canopy and C_D is the heat capacity of the dry canopy. The heat capacity of the canopy is calculated according to the formula

$$C_D = c_w (b_0 + b_1 \bar{L} + b_2 \bar{L}^2), \quad (18)$$

where b_0 , b_1 , and b_2 are constants with dimensions of length and \bar{L} is the time average of the leaf area index.

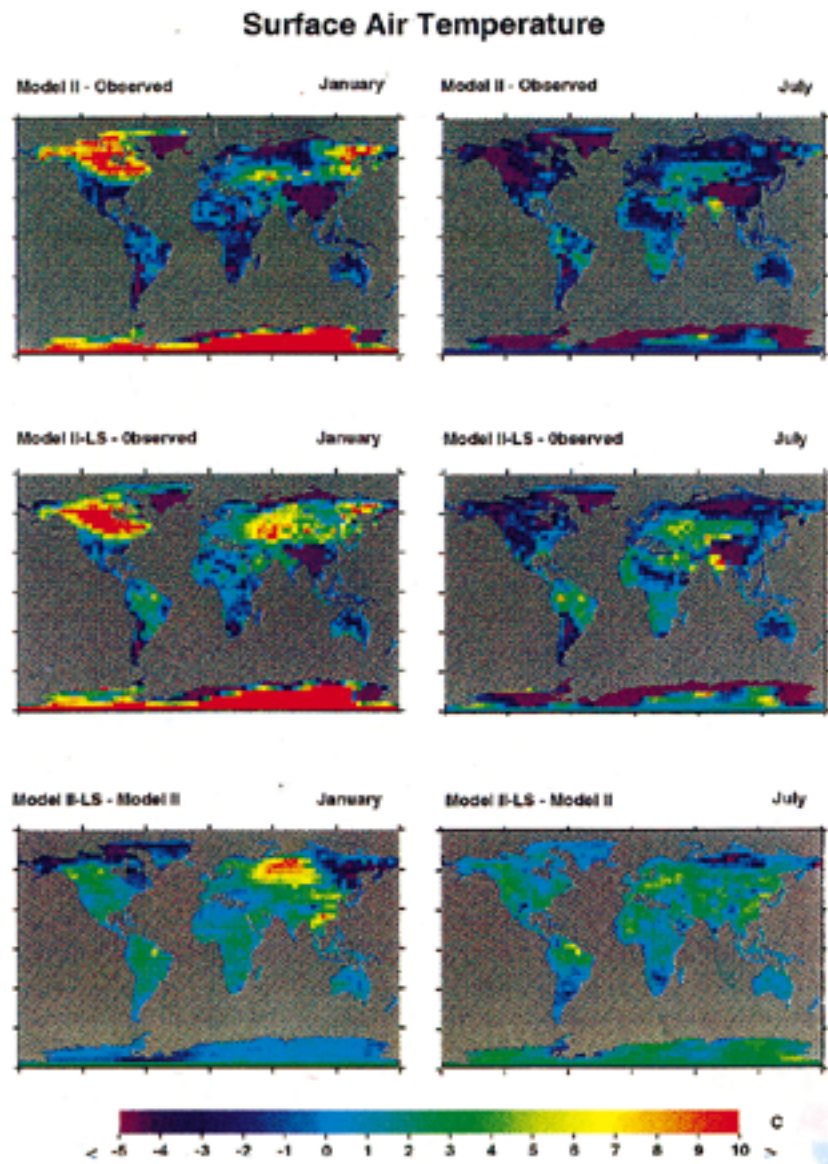


FIG. 3. Differences in simulated and observed January and July surface air temperature for GISS Model II and Model II-LS. Observations are from Legates and Willmott (1990a).

6) METHOD OF SOLUTION

Because canopy heat is a prognostic variable, T_G is known at the beginning of the time step. This value of T_G is combined with the atmospheric layer 1 quantities to solve for T_s and the surface wind velocity by using the GCM surface routine. Then, q_s is obtained by using (15). Finally, all the fluxes are determined as described in section 2c(1).

d. Soil and vegetation properties

Soil and vegetation properties are based on $1^\circ \times 1^\circ$ databases and composited to grid-box resolution.

1) SOIL CLASSIFICATION, CHARACTERISTICS, AND LAYERS

The Zobler world soil data file (Zobler 1986) prescribes soil units and surface slope at a $1^\circ \text{ lat} \times 1^\circ \text{ long}$ resolution according to the United Nations Food and Agriculture Organization–United Nations Educational, Scientific, and Cultural Organization (FAO–UNESCO) soil maps (FAO–UNESCO 1971–1981). Another global database specifies soil horizon thicknesses and textures (particle size distributions) at a $1^\circ \text{ lat} \times 1^\circ \text{ long}$ resolution (Webb et al. 1991, 1993) based on selected soil profiles and information included with the FAO soil maps (FAO–UNESCO 1971–1981, 1988). The latter

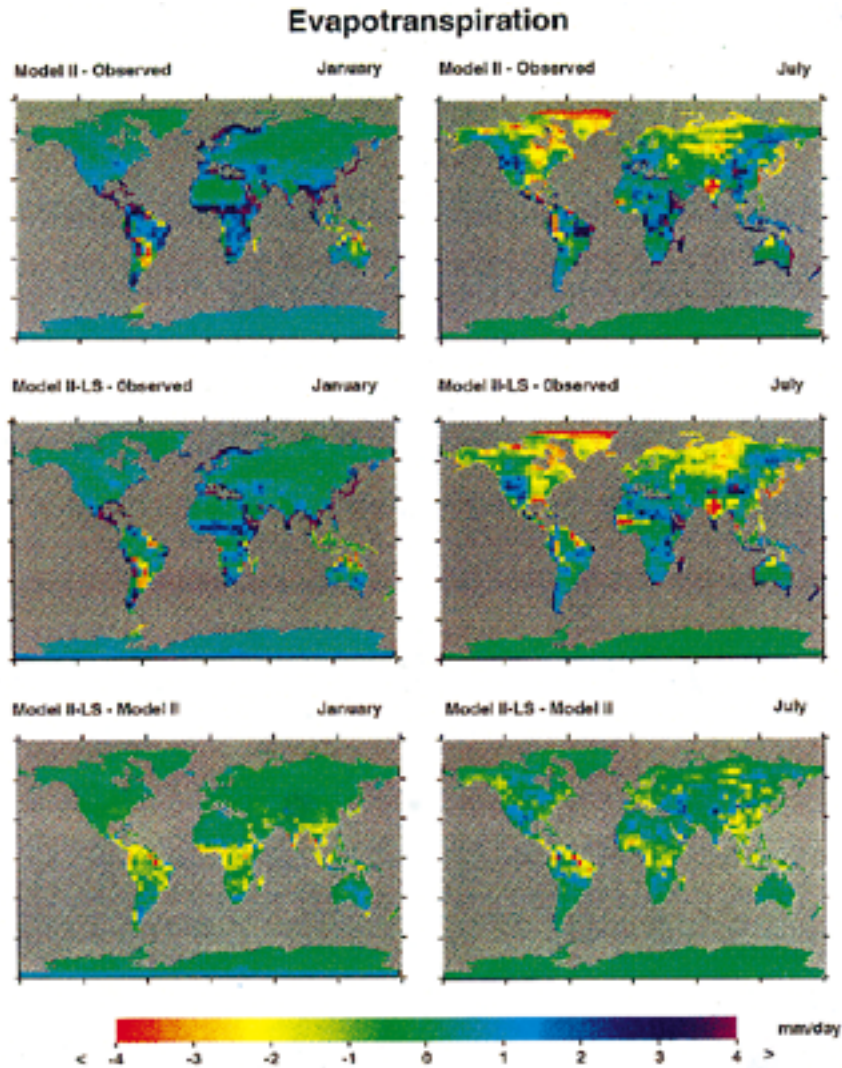


FIG. 4. Differences in simulated and observed January and July evapotranspiration for GISS Model II and Model II-LS. Observations are from Willmott et al. (1985).

database contains the top and bottom depths and the percentages of the abundance of sand, loam, clay, and peat of individual soil horizons in each of 106 soil types, differentiated for nine continental divisions. The weighted average of surface slopes within a grid box is used to calculate underground runoff.

The GCM layer thicknesses were chosen to be geometrically increasing, with the bottom boundary terminating at a depth of 3.5 m. There are six soil layers, with the thickness of the first layer specified as 0.1 m. The fraction of volume of each soil texture within each GCM layer is then totaled. If some of the $1^\circ \text{ lat} \times 1^\circ$ long grid boxes that compose the GCM layer contain bedrock at that depth, then this bedrock volume is added to the GCM layer as though it were another texture.

The equipotential value of matric potential is found over the different texture components (excluding bed-

rock) of the soil layer based on the total moisture content of the layer. The diffusivity and conductivity of the layer are then calculated by taking the weighted average of their values over the individual textures at the given matric potential. For soil water movement, the gravitational potential is included in the calculations.

2) VEGETATION CLASSIFICATION, PROPERTIES, AND SEASONALITY

Eight vegetation types are prescribed as in GISS Model II (Hansen et al. 1983; Matthews 1983, 1984).¹ The

¹ A new category, cultivated land, has been added recently, as well as two categories of bare soil, which are differentiated by albedo (E. Matthews 1994, personal communication). The results reported in this paper do not include the new land categories.

TABLE 2. Means and root-mean-square deviations of climate variables averaged over global land-surface area for observations and GCM model development runs.

A. Means						
Variable	Obs*	Model II	Model II LS	Model II LS'	Model II CON and PBL	Model II LS, CON, and PBL
January						
Precipitation (mm day ⁻¹)	2.19	2.68	2.56	2.56	2.37	2.47
Evaporation (mm day ⁻¹)	0.96	1.96	1.59	1.62	1.55	1.67
Surface air temperature (°C)	3.4	3.4	4.9	4.8	3.8	3.5
Std dev surface air temp (°C)**						
Diurnal surface air Temperature range (°C)	9.7	9.7	8.9	10.5	11.1	7.9
July						
Precipitation (mm day ⁻¹)	2.56	2.84	2.66	2.64	2.64	2.88
Evaporation (mm day ⁻¹)	2.10	2.35	2.08	2.07	2.03	2.27
Surface air temperature (°C)	14.5	12.7	14.2	13.7	14.5	13.5
Std dev surface air temperature (°C)**	0.60	0.65	0.72	0.66	0.91	0.90
Diurnal surface air Temperature range (°C)	10.9	12.4	10.4	12.3	14.9	9.9
B. Root-mean-square deviations						
Variable*	Model II	Model II LS	Model II LS'	Model II CON and PBL	Model II ILS, CON, and PBL	
January						
Precipitation (mm day ⁻¹)	2.29	2.38	2.30	1.98	1.92	
Evaporation (mm day ⁻¹)	1.78	1.44	1.41	1.22	1.25	
Surface air temperature (°C)	4.10	4.45	3.97	4.03	4.67	
Std dev surface air temperature (°C)**						
Diurnal surface air Temperature range (°C)	3.27	3.07	2.95	4.83	3.68	
July						
Precipitation (mm day ⁻¹)	2.58	2.84	2.78	3.00	2.84	
Evaporation (mm day ⁻¹)	1.63	1.49	1.46	1.47	1.51	
Surface air temperature (°C)	7.98	7.74	7.69	7.08	6.92	
Std dev surface air temperature (°C)**	0.53	0.47	0.42	0.62	0.63	
Diurnal surface air Temperature range (°C)	3.94	3.11	3.30	6.74	3.30	

* Observation sources: precipitation—Legates and Willmott (1990b), evaporation—Willmott et al. (1985), surface air temperature—Oort (1983), Std dev surface air temperature—J. Hansen et al. (1994, personal communication), and diurnal surface air temperature range—May et al. (1992).

** June–July–August.

fraction of bare soil is taken to be the amount of the “desert” vegetation type in each grid box. For each vegetation type, the following properties are specified: leaf area index, minimum stomatal resistance, maximum vegetation height, and root density and depth (Table 1). Vegetation characteristics are specified from the literature to represent generic functioning. For example, we specify a rainforest root depth of 0.8 m to account for the major concentration of roots near the surface in this vegetation type, even though root depths may extend up to 4 m or deeper (Gash et al. 1996). Weighted averages of the characteristics are calculated over the different vegetation types within a grid box.

Seasonality in vegetation is simulated by representing the leaf area index as a sinusoidally varying function of time. For each vegetation type, a different amplitude, mean, and phase are described. Opposite phases are

specified for the Northern and Southern Hemispheres; vegetation types in the Tropics display less difference between minimum and maximum leaf area index and, therefore, less seasonality.

3. Results

Model II-LS primarily influences the surface air temperature over land, both in monthly means and diurnal range, and affects the major components of the hydrologic cycle over land—evapotranspiration, runoff, and precipitation—as simulated by the GISS GCM Model II. No effort was made to adjust the model parameters such as interstream distance or canopy water-holding capacity. Such values may be adjusted in future simulations to give more realistic results.

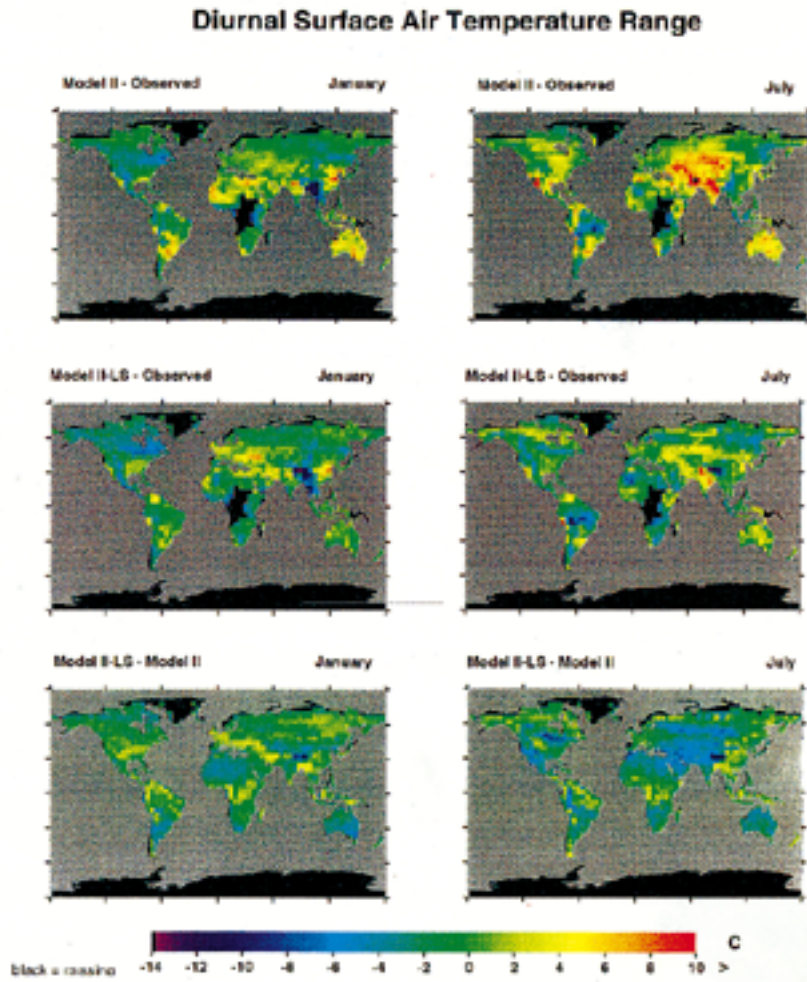


FIG. 5. Differences in simulated and observed January and July diurnal surface air temperature range for GISS GCM Model II and Model II-LS. Observations are from May et al. (1992).

a. Surface air temperature

Figure 3 shows comparisons of January and July surface air temperature simulated by Model II and Model II-LS with observations (Legates and Willmott 1990a) and with each other. Both models produce excessively warm surface air temperature in the Northern Hemisphere winter. The current LS snow formulation may contribute to this problem when snow depths are large. If there is a single thick snow layer, the large heat capacity of the snow negates the model's representation of the insulating effect of snow, which occurs only between the first and second soil layers. This inhibits the fluctuation of the temperature at the top of the snow, possibly leading to high air temperatures in winter. The inclusion of an explicit three-layer snow model with associated snow depths, snow water equivalents, and snowpack densities may correct this deficiency (Lynch-Stieglitz 1994).

It should be noted that the land-surface model does

not include Antarctica, which is modeled in the GCM by the land ice routines. In Fig. 3, Antarctica shows the opposite error than the Northern Hemisphere; that is, it is too cold in the winter and too hot in the summer.

Model II-LS simulates higher surface air temperature than Model II in both January and July in most locations. This difference is most noticeable in north-central Asia in winter. The overall increase in temperature in Model II-LS is probably due to the inclusion of explicit canopy resistance, which results in lower evaporation in many locations (Fig. 4; Table 2), and thus lower latent heat and higher sensible heat fluxes. Model II-LS improves the simulation of surface air temperature in Africa in January, and in North America, Europe, and Africa in July. However, Model II-LS does not correct Model II's excessively cool surface air temperature in Southeast Asia and errs in simulating temperatures that are too high in southwest and central Asia, effects possibly due to artificially high canopy heat capacities and/or errors

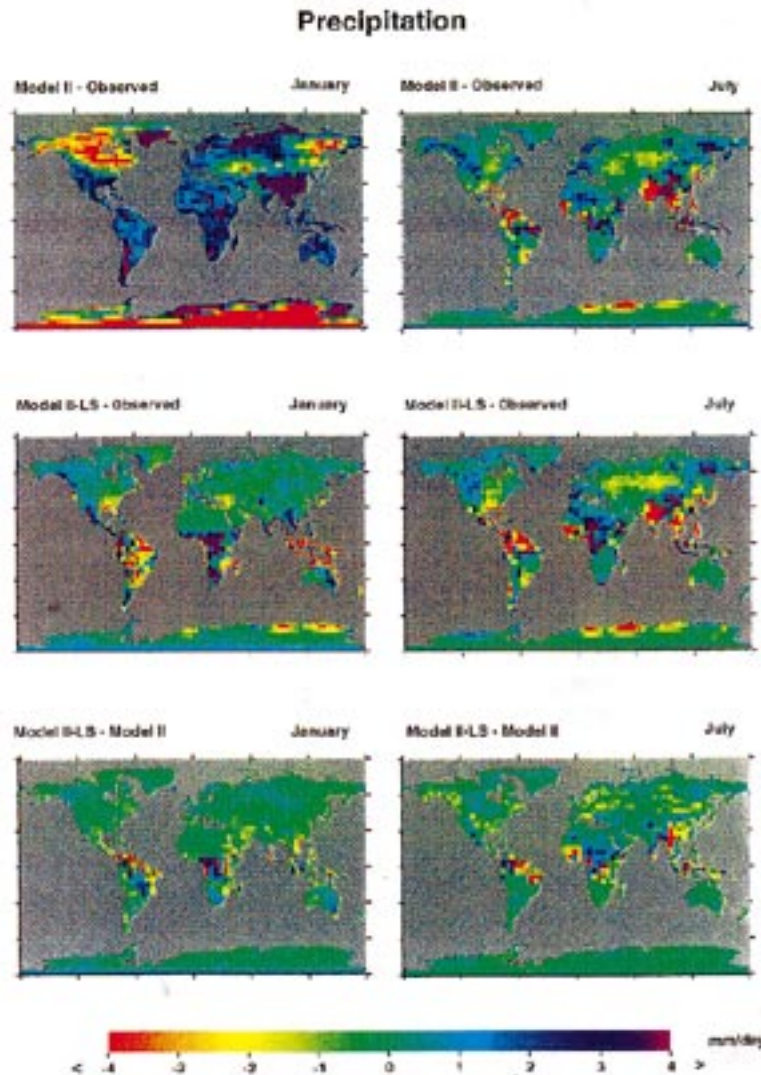


FIG. 6. Differences in simulated and observed January and July precipitation for GISS GCM Model II and Model II-LS. Observations are from Legates and Willmott (1990b).

in large-scale winds in these regions. Model II-LS also reduces the rms error of surface air temperature variability in summer, expressed as the year-to-year standard deviation of mean summer temperature (Table 2).

b. Diurnal surface air temperature range

Model II uses a modified bucket scheme for soil water calculations and neglects vegetative canopy resistance to evaporation. In some land areas, excess evaporation leads to soil drying early in the summer, causing the diurnal surface air temperature range to be high (Fig. 5). This effect can be seen in the diurnal surface air temperature range simulated by Model II in southwest Asia in July compared to observations by May et al. (1992). Contributing factors to this result include the

diminishing of the cooling effect of latent heat flux and the lower heat capacity of dry soil. Model II-LS improves the results by simulating groundwater and heat fluxes more accurately, thereby lowering the simulated diurnal surface air temperature range in many regions. However, the range is still too high in many other regions.

c. Precipitation

Figure 6 shows comparisons of January and July precipitation simulated by Model II and Model II-LS with observations (Legates and Willmott 1990b) and with each other. Model II-LS tends to decrease precipitation in low latitudes (except in central Africa) and in summer in the Northern Hemisphere compared to Model II, a

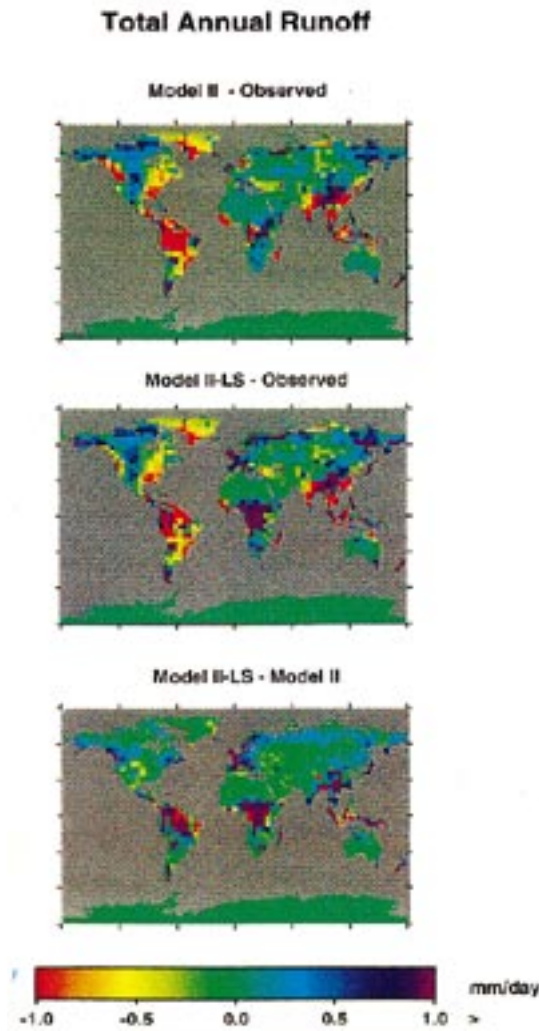


FIG. 7. Differences in simulated and observed annual total runoff for GISS GCM Model II and Model II-LS. Observations are from Korzun et al. (1977).

result that may be linked to the decrease in evapotranspiration shown in Fig. 4. However, precipitation in the GCM depends on many other factors besides the land-surface parameterization.

d. Runoff

Annual differences between simulated and observed runoff and between Model II-LS and Model II at 4° lat \times 5° long resolution are shown in Fig. 7 (Korzun et al. 1977). The land-surface parameterization of Model II-LS generally increases runoff values due to the inclusion of underground as well as surface runoff. While Model II-LS increases runoff in northwest North America, thereby improving the simulation, it fails to locate the peak runoff in East Africa, where the Congo River is located. High runoff is predicted instead in central

Africa, where model precipitation is too high. Simulation of river flow in the Amazon Basin, which was very low in Model II, significantly improves (Marengo et al. 1994). This occurs because Model II-LS produces lower, more realistic evaporation over the Amazon Basin, leading to increases in runoff. A river flow routing scheme (Russell and Miller 1990; Miller et al. 1994) will be used to calibrate the parameters for interstream distance and surface crusting in Model II-LS in the 33 major river basins of the world analyzed by Russell and Miller (1990).

e. Models II-LS and II-LS'

Initially we used $b_0 = 0.010m$, $b_1 = 0.002m$, and $b_2 = 0.001m$ as the coefficients in (18) to specify the Model II-LS canopy heat capacity. We found that these coefficients produced high heat capacities (ranging from $5.89 \times 10^4 \text{ J m}^{-2} \text{ }^\circ\text{C}^{-1}$ for tundra to $4.56 \times 10^5 \text{ J m}^{-2} \text{ }^\circ\text{C}^{-1}$ for evergreen forest) and contributed to excessively high summer temperatures in central Asia in July. We then tried running the II-LS model with the heat capacities all reduced by a factor of 10; this resulted in canopy heat capacities for forests that are closer to those derived by Thom (1975). Reducing the canopy heat capacities reduced the summer temperatures in Asia to more acceptable levels, but increased the computation time on the order of 60% due to the reduction of the internal time-step to avoid oscillation. The results in Table 2 indicated by II-LS refer to the initial, higher canopy heat capacities, and those indicated by II-LS' refer to the reduced canopy heat capacities.

The reduction in July average temperatures in Model II-LS' compared to Model II-LS can be explained by the fact that canopies with lower heat capacity tend to have larger diurnal temperature ranges. Because the peak diurnal canopy temperatures are higher, latent and sensible heat fluxes are greater. Canopy fluxes are not as affected by the low end of the diurnal temperature range, where the atmosphere tends to be more stable. Overall, there is a net increase in the upward sensible and latent heat fluxes for the lower canopy heat capacity, thus reducing the average canopy temperature.

f. Interaction with other model components

Development of the land-surface component of the GISS GCM is proceeding simultaneously with improvements in other GCM components (Marengo and Druyan 1994). Table 2 shows observed and simulated means and root-mean-square deviation values for observed and simulated climate variables over the global land surface. The models compared are the GISS GCM II; Model II-LS; Model II-PBL-CON, with improved planetary boundary layer and convection schemes (Hartke and Rind 1996; Del Genio and Yao 1988, 1993; Del Genio et al. 1996); and Model II-LS-PBL-CON, with all three improvements (land surface, planetary boundary layer,

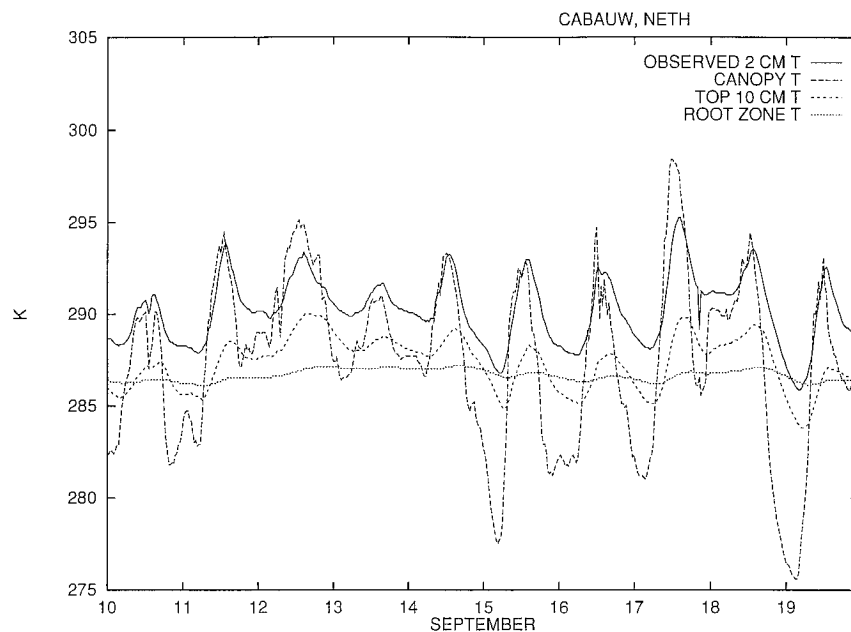


FIG. 8. Observed 2-cm soil temperature and simulated canopy temperature, soil temperature of top 10 cm, and root zone temperature, for 10–19 September 1987 at Cabauw, Netherlands. Data from Beljaars (1982) and Project for Intercomparison of Land-Surface Parameterization Schemes (PILPS).

and convection). All model runs were carried out at $4^\circ \times 5^\circ$ resolution. It is important to note that the GISS Model II has undergone more calibration of parameters than have the other three models.

Models II-LS, II-PBL, and II-CON tend to improve the global means of some, but not all, of the climate variables analyzed. The land-surface parameterization improves the January means of precipitation and evaporation; in July, the land-surface model improves precipitation, evaporation, surface air temperature, and diurnal surface air temperature range. The combination of all three new routines improves the January mean precipitation and evaporation; in July, the combined model improves the mean evaporation, surface air temperature, and diurnal surface air temperature range.

The land-surface parameterizations (LS and LS') improve the root-mean-squares of diurnal surface air temperature range in January; surface air temperature and diurnal surface air temperature range are improved in July.

The simulation with the other two model components (CON and PBL) improves the rms of three climate variables in January and two in July. The July simulation of the diurnal surface air temperature range is especially poor. When all three model schemes are combined, two and three climate variables are improved in the January and July simulations, respectively. Diurnal surface air temperature range is especially improved in July when the land-surface model is included. Evaporation is improved in both January and July in the three-way combination.

These improvements indicate that the land-surface parameterization described here should, in general, provide a more realistic simulation of climate variables over land in conjunction with other improvements to the GISS GCM.

g. Land-surface model intercomparison

Phase 2 of PILPS involved the offline simulation and validation of land-surface fluxes for a grassland site in Cabauw, the Netherlands. Figures 8 and 9 show the simulated and observed (Beljaars 1982; Holtslag and van Ulden 1983) hourly temperature and latent and sensible heat flux data for 10 days in September. The LS' version of the land-surface model was used for the Cabauw experiment.

The variations of observed ground temperature at 2-cm depth lie between those of the simulated canopy temperature and the simulated ground temperature at 10 cm, while the simulated root zone temperature remains almost constant (Fig. 8). This result shows that the model simulates the ground temperature lag with depth in a reasonable way. The larger swings in the canopy temperature are expected due to its lower heat capacity.

When simulated latent and sensible heat fluxes are compared with observations, the GISS LS' model tends to underestimate latent heat fluxes and overestimate sensible heat fluxes (Fig. 9). This result may indicate lack of realism in the modeling of the controls on the canopy resistance. Low soil moisture or high air temperature may be causing latent heat flux to be curtailed in the

model, leading to a concurrent rise in simulated sensible heat. The modeled boundary layer resistance may also be too low, which would enhance the control of the canopy resistance.

Alternatively, since the Cabauw “observations” of sensible and latent heat are not direct measurements, errors may be present due to the estimation of these quantities. The sensible heat was derived from observed temperature and wind profiles using a flux-profile parameterization; latent heat was derived from the residual of the surface energy balance (Beljaars 1982). Furthermore, missing data were filled in using another parameterization scheme (Holtslag and van Ulden 1983). In particular, the Beljaars coefficient of drag under stable atmospheric conditions (i.e., usually at night) appears to be consistently higher than that of the GISS Model II parameterization. This has the effect of producing greater downward sensible heat fluxes at night in the PILPS Cabauw dataset compared to the GISS LS’.

4. Conclusions

The model development described herein seeks to provide a more realistic yet still simple calculation of land-surface processes for the GISS GCM based on physical principles. The results presented in this paper show that the inclusion of more physically realistic processes improves simulation of land-surface fluxes for some variables in some locations and in some seasons, but improvements are by no means ubiquitous nor uniform among seasons. The combination of the land-surface model with improved parameterizations of other processes gives better overall improvement in global climate simulations, implying that progress in climate modeling requires a coordination of effort.

The new land-surface model contributes to a more accurate assessment of water availability changes in a warming climate, a prime motivation for the improved parameterization. The model also contributes to a better understanding of the interrelated earth system impacts of other global change processes such as deforestation and land degradation, shifts in vegetation with warming, and salinity changes in the ocean from changes in river runoff.

Future model development will include more detailed simulation of snow and runoff. We plan to include subgrid-scale soil moisture generated topographically, such that horizontal convergence of base flow into lowlands supports and maintains the saturated zones (Stieglitz et al. 1997). This incorporates techniques used in basin-scale hydrologic modeling and should further improve runoff simulation in the GISS GCM. Intermodel comparisons (e.g., PILPS) and validation with datasets provided by combined field and satellite data collection programs [e.g., the Hydrological Atmospheric Pilot Experiment, the Boreal Ecosystem–Atmosphere Study, and the Global Energy and Water Cycle Experiment (GEW-

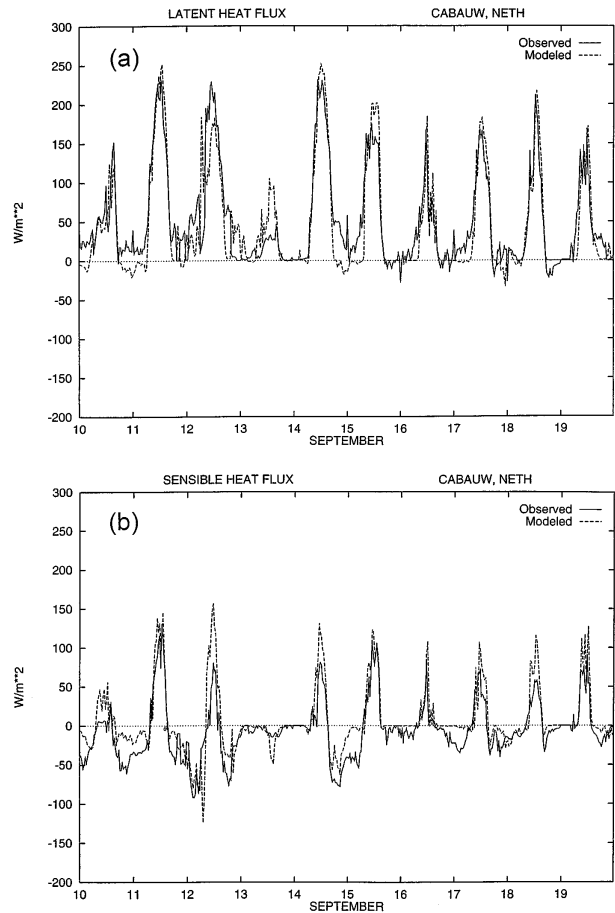


FIG. 9. Simulated (a) and observed (b) latent and sensible heat fluxes for 10–19 September 1987 at Cabauw, the Netherlands. Data from Beljaars (1982) and Project for Intercomparison of Land-Surface Parameterization Schemes (PILPS).

EX) Continental-Scale International Project] are essential.

Acknowledgments. We thank David Rind and Daniel Hillel for ongoing scientific collaboration, Jean Lerner for her help with validation datasets, and Katie Gallagher and Rich Goldberg for producing the graphics. The runoff data were digitized by P. Schulz of Research and Data Systems Corporation, NOAA/Climate Analysis Center, Camp Springs, Maryland. This work was supported by the NASA Climate Program.

APPENDIX

Symbols

b_i	Coefficients for canopy heat capacity
c_i	Stomatal resistance coefficients
C_a	Atmospheric conductance
C_c	Canopy conductance
C_D	Heat capacity of the dry canopy
C_L	Heat capacity of dry soil layer
c_i	Specific heat capacity of ice

c_w	Specific heat of water
F_H	Soil heat flux
F_{h1}	Sensible heat flux from the surface layer to the first layer in the atmosphere.
F_{hb}	Sensible heat flux from bare soil
F_{hd}	Throughfall heat flux
F_{hp}	Precipitation heat flux
F_{hv}	Sensible heat flux from the canopy
F_{q1}	Moisture flux from the surface layer to the first layer in the atmosphere
F_{qb}	Moisture flux from bare soil
F_{qv}	Moisture flux from the canopy
f_B	Fraction of grid box that is bare soil
f_P	Fraction of grid box containing convective precipitation
f_s	Fraction of canopy covered with snow
f_V	Fraction of grid box that is vegetated
G_s	Specific gravity of snow
H_C	Heat content of the canopy
H_L	Heat in a soil layer
h_f	Heat of fusion of water
I	Incoming solar radiation
I_L	Ice in a soil layer
K	Eddy diffusion coefficient
K_H	Soil thermal conductivity
L	Leaf area index
L_{eff}	Effective leaf area index
N	Infiltration capacity
P	Precipitation
P_C	Maximum precipitation that can fall in a given period without throughfall
P_V	Throughfall
q_1	Water vapor mixing ratio in the first layer of the atmosphere
q_B	Saturated water vapor mixing ratio at the temperature of bare soil
q_C	Saturated water vapor mixing ratio at the temperature of the canopy
q_s	Water vapor mixing ratio in the surface layer
R	Runoff
R_{nc}	Net radiation of the canopy
r_s	Minimum stomatal resistance
S	Water equivalent snow depth
T	Soil temperature
T_1	Temperature of the first layer of the atmosphere
T_B	Temperature of bare ground
T_C	Canopy temperature
T_G	Effective ground temperature
T_L	Temperature of a soil layer
T_S	Surface temperature
V_h	Vegetation height
W_C	Water content of the canopy
W_L	Water in a soil layer
Z_1	Height of the first layer of the atmosphere
Z_S	Height of surface layer
z	Vertical coordinate in soil
β_B	Soil moisture availability in bare soil
β_D	Soil water availability in the vegetated portion of the grid box
β_V	Overall evaporative efficiency for the canopy
λ	Latent heat of evaporation

REFERENCES

- Abramopoulos, F., C. Rosenzweig, and B. Choudhury, 1988: Improved ground hydrology calculations for global climate models (GCMs): Soil water movement and evapotranspiration. *J. Climate*, **1**, 921–941.
- Beljaars, A. C. M., 1982: The derivation of fluxes from profiles in perturbed areas. *Bound.-Layer Meteor.*, **24**, 35–55.
- Deardorff, J. W., 1978: Efficient prediction of ground surface temperature and moisture, with inclusion of a layer of vegetation. *J. Geophys. Res.*, **83**, 1889–1903.
- Del Genio, A. D., and M.-S. Yao, 1988: Sensitivity of a global climate model to the specification of convective updraft and down-draft mass fluxes. *J. Atmos. Sci.*, **45**, 2641–2667.
- , and —, 1993: Efficient cumulus parameterization for long-term, climate studies: The GISS scheme. *The Representation of Cumulus Convection in Numerical Models, Meteor. Monogr.*, No. 46, Amer. Meteor. Soc., 181–124.
- , —, W. Kovari, and K. K.-W. Lo, 1996: prognostic cloud water parameterization for global climate models. *J. Climate*, **9**, 270–304.
- De Vries, D. A., 1966: Thermal properties of soils. *Physics of Plant Environment*, W. R. van Wijk, Ed., North-Holland Publishing, 210–235.
- Dickinson, R. E., 1984: Modeling evapotranspiration for three-dimensional global climate models. *Climate Processes and Climate Sensitivity*, J. E. Hansen and T. Takahashi, Eds., Amer. Geophys. Union, 58–72.
- Eltahir, E. A. B., and R. L. Bras, 1993: Estimation of the fractional coverage of rainfall in climate models. *J. Climate*, **6**, 639–644.
- Entekhabi, D., and P. S. Eagleson, 1989: Land surface hydrology parameterization for atmospheric general circulation models including subgrid scale spatial variability. *J. Climate*, **2**, 816–829.
- FAO-UNESCO, 1971–1981: *Soil Map of the World, 1:5,000,000*. Vols. I-X, UNESCO.
- , 1988. Soil map of the world: Revised legend. World Resources Rep. 60, 138 pp. [Available from FAO, Via delle Terme di Caracalla, 00100 Rome, Italy.]
- Gardner, W. R., and D. Hillel, 1962: The relation of external evaporative conditions to the drying of soils. *J. Geophys. Res.*, **67**, 4319–4325.
- Gash, J. H. C., C. A. Nobre, J. M. Roberts, R. L. Victoria, Eds., 1996: *Amazonian Deforestation and Climate*. John Wiley, 430 pp.
- Hansen, J., G. L. Russell, D. Rind, P. Stone, A. Lacis, S. Lebedeff, R. A. Ruedy, and L. Travis, 1983: Efficient three-dimensional global models for climate studies: Models I and II. *Mon. Wea. Rev.*, **111**, 609–683.
- Hartke, G. J., and D. Rind, 1996: Improved surface and boundary layer models for the GISS GCM. *J. Geophys. Res.*, in press.
- Henderson-Sellers, A., and R. E. Dickinson, 1992: Intercomparison of land-surface parameterizations launched. *Eos, Trans. Amer. Geophys. Union*, **73**, 195–196.
- , A. J. Pitman, P. K. Love, P. Irannejad, and T. H. Chen, 1995: The Project for Intercomparison of Land Surface Parameterization Schemes (PILPS): Phases 2 and 3. *Bull. Amer. Meteor. Soc.*, **76**, 489–503.
- Hillel, D., 1975: Evaporation from bare soil under constant and diurnally fluctuating evaporativity. *Soil Sci.*, **120**, 230–237.
- Holtslag, A. A. M., and A. P. van Ulden, 1983: A simple scheme for daytime estimates of the surface fluxes from routine weather data. *J. Climate Appl. Meteor.*, **22**, 517–529.
- Korzun, V. I., A. A. Sokolov, M. I. Budyko, K. P. Voskresensky, G. P. Kalinin, A. A. Konovlyantsev, E. S. Korotkevich, and M. I. Lvovich, Eds., 1977: *Atlas of World Water Balance*. USSR National Committee for the International Hydrological Decade, UNESCO Press, 663 pp.
- Legates, D. R., and C. J. Willmott, 1990a: Mean seasonal and spatial variability in global surface air temperature. *J. Theor. Appl. Climatol.*, **41**, 11–21.
- , and —, 1990b: Mean seasonal and spatial variability in gauge-corrected, global precipitation. *Int. J. Climatol.*, **10**, 111–127.
- Lynch-Stieglitz, M., 1994: The development and validation of a simple snow model for the GISS GCM. *J. Climate*, **7**, 1842–1855.

- Marengo, J., and L. Druyan, 1994: Validation of model improvements for the GISS GCM. *Climate Dyn.*, **10**, 163–179.
- , J. R. Miller, G. L. Russell, C. E. Rosenzweig, and F. Abramopoulos, 1994: Calculations of river-runoff in the GISS-GCM: Impact of a new land-surface and a runoff routing model on the hydrology of the Amazon River. *Climate Dyn.*, **10**, 349–361.
- Mathews, E., 1983: Global vegetation and land use: New high-resolution data bases for climate studies. *J. Climate Appl. Meteor.*, **22**, 474–487.
- , 1984: Prescription of land-surface boundary conditions in GISS GCM II: A simple method based on high-resolution vegetation data bases. NASA Tech. Memo. 86096, 20 pp. National Aeronautics and Space Administration, Greenbelt, MD, 20 pp. [Available from NTIS, Springfield, VA 22161.]
- May, W., D. J. Shea, and R. A. Madden, 1992: The annual variation of surface temperatures over the world. NCAR Tech. Note NCAR/TN-372+STR, National Center for Atmospheric Research, Boulder, CO, 145 pp. [Available from NCAR, Information Services, Boulder, CO 80301.]
- Miller, J. R., G. Russell, and G. Caliri, 1994: Continental scale river flow in climate models. *J. Climate*, **7**, 914–928.
- Neeman, B. U., J. H. Joseph, and G. Ohring, 1988: A vertically integrated snow/ice model over land/sea for climate models: I. Development. *J. Geophys. Res.*, **93**, 3663–3675.
- Oort, A., 1983: Global atmospheric circulation statistics, 1958–1973. NOAA. Prof. Paper 14, 180 pp. [Available from NTIS, Springfield, VA 22161.]
- Russell, G., and J. Miller, 1990: Global river runoff calculated from a global atmospheric general circulation model. *J. Hydrol.*, **117**, 241–254.
- Sellers, P. J., Y. Mintz, Y. C. Sud, and A. Dalcher, 1986: A simple biosphere (SiB) for use within general circulation models. *J. Atmos. Sci.*, **43**, 505–531.
- Steiglitz, M., D. Rind, J. Famiglietti, and C. Rosenzweig, 1997: An efficient approach to modeling the topographic control of surface hydrology for regional and global climate modeling. *J. Climate*, **10**, 118–137.
- Thom, A. S., 1975: Momentum, mass and heat exchange of plant communities. *Vegetation and the Atmosphere*. Vol. 1, *Principles*, J. L. Monteith, Ed., Academic Press, 57–109.
- Webb, R. S., C. Rosenzweig, and E. R. Levine, 1991: A global data set of soil particle size properties. NASA Tech. Memo. 4286, National Aeronautics and Space Administration, Greenbelt, MD, 33 pp. [Available from NTIS, Springfield, VA 22161.]
- , —, and —, 1993: Specifying land-surface characteristics in general circulation models: Soil profile data set and derived water-holding capacities. *Global Biogeochem. Cycles*, **7**, 97–108.
- Willmott, C., M. Rowe, and Y. Mintz, 1985: Climatology of the terrestrial seasonal water cycle. *J. Climatol.*, **5**, 589–606.
- Zobler, L., 1986: A world soil file for global climate modeling. NASA Tech. Memo. 87802, National Aeronautics and Space Administration, Greenbelt, MD, 32 pp. [Available from NTIS, Springfield, VA 22161.]